

Tomographic Image Reconstruction using Dictionary Priors

Sara Soltani ^{*}, Martin S. Andersen [†] and Per Christian Hansen [‡]

Department of Applied Mathematics and Computer Science,
Technical University of Denmark, DK-2800 Kgs. Lyngby,
Denmark.

July 21, 2022

Abstract

We describe and examine a framework for tomographic image reconstruction where prior knowledge about the solution is available in the form of training images. We first construct a dictionary that contains prototype elements from these images. Then by using the dictionary as a prior to regularize the inverse problem, and looking for a solution with a sparse representation in the dictionary, we formulate the reconstruction problem in a convex optimization framework. Our computational experiments clarify the choice and interplay of the model parameters and the regularization parameters, and they show that in few-projection settings we are able to produce better images with more structural features than the total variation approach.

1 Introduction

In computed tomography (CT) it is challenging to obtain sharp and reliable reconstructions when using few projections or a limited-angle setting (e.g., due to measurement or dose constraints). These limited-data scenarios lead to underdetermined problems and classical reconstruction methods, such as filtered back projection or algebraic reconstruction techniques, are often incapable of producing satisfactory reconstructions because they fail to incorporate adequate prior information (see, e.g., [3]).

To overcome these difficulties it is necessary to incorporate a strong prior about the solution that can compensate for the lack of data. One such prior

^{*}ssol@dtu.dk

[†]mkan@dtu.dk

[‡]pcha@dtu.dk

This work is part of the project HD-Tomo funded by Advanced Grant No. 291405 from the European Research Council

2010 Mathematics Subject Classification: Primary: 65F22; Secondary: 65K10.

Key words and Phrases: Tomography, Dictionary learning, Inverse problem, Regularization, Sparse representation, Image reconstruction.

is that the solution is piecewise constant, leading to total variation (TV) regularization schemes [17], [31]. These methods can be very powerful when the solution is approximately composed of homogeneous regions separated by sharp boundaries.

An alternative approach is to use prior information in the form of “training images” that characterize the geometrical or visual features of the property of interest, e.g., from pictures of specimens or from high-accuracy reconstructions. The goal of this work is to elaborate on this approach. We study how to incorporate such priors in a two-stage framework, where the most important features of the training data is extracted and then integrated in the reconstruction problem formulation.

The natural way to incorporate prior information from training images is to form a *dictionary* that sparsely encodes the information [25]. Learning the dictionary from given training data appears to be very suited for incorporating priors that are otherwise difficult to formulate in a closed form, such as image texture.

Sparse representation of signals and images has acquired a great deal of interest and has been extensively studied in recent years (see, e.g., [8] and [30]), and dictionary learning is now used in many areas including image denoising [6], [20], inpainting [23], and deblurring [22]. Elad and Ahron [9] address the image denoising problem using a process that combines dictionary learning and reconstruction. They consider the use of a dictionary trained from a noise-free image using the K-SVD algorithm [1], as well as an adaptive dictionary trained on patches of the noisy image.

The use of dictionary learning in tomographic imaging has also emerged recently. In [21] and [26], in the absence of training images, the tomographic reconstruction is computed using an alternating minimization procedure where the dictionary is learned from intermediate solutions. Inspired by [9], Xu and Yu [32] presented a mathematical framework for low-dose CT reconstruction where they learn a dictionary either from high-resolution images (using the online dictionary learning method [24]) or from intermediate images obtained when solving the reconstruction problem iteratively.

Etter, Jovanović, and Vetterli [11] also considered a two-stage approach where a dictionary is learned by means of the K-SVD algorithm, and then a least squares reconstruction is expressed as a linear combination of the columns of the dictionary. Their algorithm is tested on a simple tomography setup with no noise in the data. An ultrasound tomography problem was considered in [29], where the dictionary is learned from a large set of MRI breast tissue scans using an unsupervised maximum likelihood dictionary learning method. It is demonstrated that the use of a learned dictionary improves the reconstruction over a wavelet-based approach.

Simultaneous learning and reconstruction, where the dictionary is learned from the given data, is an NP hard problem and it is unclear how the properties of the dictionary influence the computed reconstruction. Furthermore, since the prior is data-driven, it violates a fundamental principle of inverse problems where data-independent prior information is incorporated to eliminate unreasonable models that fits the data.

For the above reasons we prefer to separate the two steps – which clearly works only when reliable training images are available. We describe and examine a two-stage framework where we first construct a dictionary that contains

prototype elements from these images, and then we use the dictionary as a prior to regularize the reconstruction problem. The main contributions of our paper are an empirical study of the effect of the parameters of the learned dictionary in solving the image reconstruction problem, and a comparison with the TV reconstruction method for few-view/limited-angle tomography problems with images that resemble “texture.” To the best of our knowledge, no comprehensive study has investigated and explored the influence of the learned dictionary structure and dictionary parameters in CT with under-determined systems.

Our paper is organized as follows. In section 2 we briefly discuss dictionary learning methods and present a framework for solving the image reconstruction problem using dictionaries, and in Section 3 we describe the implementation details of algorithm. Section 4 presents careful numerical experiments where we study the influence of the algorithm and design parameters. Section 5 summarizes our work.

We use the following notation, where A is an arbitrary matrix:

$$\|A\|_F = \left(\sum_{ij} A_{ij}^2 \right)^{1/2}, \quad \|A\|_{\text{sum}} = \sum_{ij} |A_{ij}|, \quad \|A\|_{\text{max}} = \max_{ij} |A_{ij}|.$$

A vector $g \in \mathbb{R}^n$ is a subgradient of $f : \mathbb{R}^n \rightarrow \mathbb{R}$ at $x \in \text{dom} f$ if

$$f(z) \geq f(x) + g^T(z - x) \quad \forall z \in \text{dom} f.$$

If f is convex and differentiable then its gradient at x is the subgradient, and a subgradient can exist even when f is not differentiable at x . The subdifferential $\partial f(x)$ of f at x is the set of all subgradients:

$$\partial f(x) = \{g \mid g^T(z - x) \leq f(z) - f(x), \forall z \in \text{dom} f\}.$$

A set C is called a cone if for every $x \in C$ and $\theta \geq 0$, we have $\theta x \in C$. A set C is a convex cone if it is convex and a cone.

2 The Reconstruction Framework

Linear tomographic reconstruction problems are often formulated as $Ax \approx b$ where the vector $x \in \mathbb{R}^n$ represents the unknown image, the vector $b \in \mathbb{R}^m$ is the given (usually inaccurate/noisy) data, and the matrix $A \in \mathbb{R}^{m \times n}$ represents the forward model. The dimensions of A , b , and x depend on the amount of data and how finely the image region is discretized. We are primarily concerned with underdetermined problems where $m < n$.

As mentioned in the introduction, classical reconstruction methods are not so well-suited for underdetermined problems, and it is difficult to incorporate specific priors about the solution in these methods. TV regularization can be better suited for edge-preserving imaging problems in low dose and/or few-view data sets; but it produces images whose pixel values are clustered into regions with somewhat constant intensity [27], with the result that textural images tend to be over-smoothed (except for the sharp edges). Another drawback is that TV tends to produce reconstructions whose intensities are incorrect [27].

Our goal is to incorporate priors – e.g., about texture – from a set of training images. We focus on formulating and finding a *learned dictionary* W from the training images and solving the tomography problem such that $x = W\alpha$

is a sparse linear combination of the dictionary elements. The sparsity underlying both the dictionary and the solution play an important role in terms of regularization.

Some works use a joint formulation that combines the dictionary learning and the reconstruction into one optimization problem, i.e., the dictionary is learned from the given noisy data. This corresponds to a “bootstrap” situation where one creates the prior as part of the solution process. Our work is different: we use a prior that is already available in the form of a set of training images, and we use this prior to stabilize the reconstruction problem. To do this, we use a two-stage algorithm where we first train the dictionary from the given training images, and then use the dictionary to compute the reconstruction. We note that the two stages are interconnected in the sense that the formulation of the learning problem affects the sparsity of the solution.

The dictionary W should comprise all the important features of the desired solution. A learned dictionary – while computationally more expensive than a fixed dictionary – has the advantage that it is tailored to the characteristics of the desired solution and optimized for the training images. Dictionary learning is a way to summarize and represent a large number of training images into fewer number of elements and, at the same time, compensate for noise or other errors in these images. In general, the learned dictionary should be robust to irrelevant features.

The number of training images should be large enough to ensure that all image features are represented, and the dictionary should preferably be overdetermined to ensure that one can sparsely realize the desired reconstructions. Using training images of the same size as the image to be reconstructed would require a huge number of training images and lead to an enormous dictionary. Therefore we must use patches of smaller size taken from the training images to train a *patch dictionary* D , and then built the *global dictionary* W from the found D .

Let the patches be of size $P \times Q$, and let the matrix $Y \in \mathbb{R}^{p \times t}$ consist of t training image patches arranged as vectors of length $p = PQ$. Then the dictionary learning problem can be viewed as the problem of approximating the training matrix as a product of two matrices, $Y \approx DH$, where $D \in \mathbb{R}^{p \times s}$ is the dictionary of s dictionary image patches (the columns of D), and $H \in \mathbb{R}^{s \times t}$ contains information about the approximation of each of the training image patches. Such a decomposition is clearly not unique, so we must incorporate further requirements to “shape” the patch dictionary D and the representation matrix H .

Imposing norm and/or non-negativity constraints on the elements of D and H or imposing sparsity constraint on matrix H are widely used in unsupervised learning. We take the same approach, and thus our generic dictionary learning problem takes the form:

$$\min_{D,H} \mathcal{L}_{\text{dic}}(Y, DH) + \Phi_{\text{dic}}(D) + \Phi_{\text{rep}}(H). \quad (1)$$

Here, the misfit of the factorization approximation is measured by the loss function \mathcal{L}_{dic} , while the priors on the patch dictionary D and the representation matrix H are taken into account by the regularization functions Φ_{dic} and Φ_{rep} .

The dictionary learning problem (1) is a non-convex optimization problem. If we choose the functions \mathcal{L}_{dic} , Φ_{dic} and Φ_{rep} to be convex, then the optimization

problem in (1) is not jointly convex in (D, H) , but it is convex with respect to each variable D or H when the other is fixed. A natural way to find a local minimum is therefore to use an alternating approach, first minimizing over H with D fixed, and then minimizing over D with H fixed.

Various dictionary learning methods proposed in the literature share the same overall structure but they consider different priors when formulating the dictionary learning problem. Examples of such methods include, but are not limited to, non-negative matrix factorization [18], the method of optimal directions [10], K-means clustering [15] and its generalization K-SVD [9], and the online dictionary learning method [24]. Recent methods for solving sparse coding dictionary learning problems are based on coordinate descent with soft thresholding [24]. The methods presented in [16] and [19], based on maximum a-posteriori probability and maximum likelihood, respectively, are dictionary learning methods designed for training data corrupted by an additive noise; this is not of interest in this work.

Having obtained the learned patch dictionary D and formed the global dictionary W , the second step is to solve the reconstruction problem. Here we find a solution $x = W\alpha$ where α solves the problem

$$\min_{\alpha} \mathcal{L}_{\text{rec}}(AW\alpha, b) + \Phi_{\text{SP}}(\alpha) + \Phi_{\text{IP}}(W\alpha), \quad (2)$$

where the data fidelity is measured by the loss function \mathcal{L}_{rec} and regularization is imposed via penalty functions. Specifically, the function Φ_{SP} enforces the Sparsity Prior on α , often formulated in terms of a sparsity inducing norm, while the function Φ_{IP} enforces the Image Prior. Presence of both priors or absence of either of these lead to different reconstructions. Given a solution α^* to (2) we compute the solution as $x^* = W\alpha^*$.

Various constraints can be imposed on the image as well as the representation. If we choose the three functions \mathcal{L}_{rec} , Φ_{SP} and Φ_{IP} to be convex, then the problem formulation (2) can be solved by means of convex optimization methods.

3 Implementation Details

Recall that the proposed framework for dictionary-based tomographic reconstruction consists of two conceptual steps: (i) computing a dictionary (using techniques from machine learning), and (ii) computing a reconstruction composed of images from the dictionary. In this section we describe one of many ways to efficiently implement such a scheme. We pose the dictionary-learning problem as a so-called non-negative sparse coding problem, and we use least squares optimization with non-negative variables and 1-norm regularization for computing a reconstruction.

3.1 The Dictionary Learning Problem

Dictionary learning problems of the form (1) are generally non-convex optimization problems because of the bilinear term DH where both D and H are variables. Applying a convergent iterative optimization method therefore does not guarantee that we find a global minimum (only a local stationary point).

To obtain a good dictionary, we must be careful when choosing the loss functions \mathcal{L}_{dic} and the penalties Φ_{dic} and Φ_{rep} on D and H , and we must also pay attention to implementation issues such as the starting point.

A non-negative matrix factorization (NMF) has the ability to extract meaningful factors [18], and with non-negative elements in D its columns represent a basis of images. Similarly, having non-negative elements in H corresponds to each training image being represented as a conic combination of dictionary images, and the representation itself is therefore non-negative. NMF often works well in combination with sparsity constraints [13] which in our application translates to training image patches being represented as a conic combination of a small number of dictionary elements (basis images).

The dictionary learning problem that we will use henceforth takes the form of non-negative sparse coding [13] of a non-negative data matrix Y :

$$\min_{D,H} \frac{1}{2} \|Y - DH\|_{\text{F}}^2 + \lambda \|H\|_{\text{sum}} \quad \text{s.t.} \quad D \in \mathcal{D}, H \in \mathbb{R}_+^{s \times t}, \quad (3)$$

where the set \mathcal{D} is compact and convex and $\lambda \geq 0$ is a regularization parameter that controls the sparsity-inducing penalty $\|H\|_{\text{sum}}$. This problem is an instance of the more general formulation (1) if we define

$$\mathcal{L}_{\text{dic}}(Y, DH) = \frac{1}{2} \|Y - DH\|_{\text{F}}^2$$

and

$$\Phi_{\text{dic}}(D) = I_{\mathcal{D}}(D), \quad \Phi_{\text{rep}}(H) = I_{\mathbb{R}_+^{s \times t}}(H) + \lambda \|H\|_{\text{sum}},$$

where $I_{\mathcal{Z}}$ denotes the indicator function of a set \mathcal{Z} . Note that the loss function is invariant under a scaling $D \mapsto tD$ and $H \mapsto t^{-1}H$ for $t > 0$. Thus, letting $t \rightarrow \infty$ implies that $\Phi_{\text{rep}}(t^{-1}H) \rightarrow 0$ and $\|tD\| \rightarrow \infty$ if D is nonzero. This means that \mathcal{D} must be compact to ensure that the problem has well-defined minima. Here we will consider two different definitions of the set \mathcal{D} , namely

$$\mathcal{D}_{\infty} \equiv \{D \in \mathbb{R}_+^{p \times s} \mid \|d_j\|_{\infty} \leq 1\} \quad \text{and} \quad \mathcal{D}_2 \equiv \{D \in \mathbb{R}_+^{p \times s} \mid \|d_j\|_2 \leq \sqrt{p}\}.$$

The set \mathcal{D}_{∞} corresponds to box constraints, and \mathcal{D}_2 is a spherical sector of the 2-norm ball with radius \sqrt{p} . As we will see in the next section, the use of \mathcal{D}_{∞} as a prior gives rise to binary-looking images (corresponding to the vertices of \mathcal{D}_{∞}) whereas \mathcal{D}_2 gives rise to more “natural looking” images.

We emphasize an important difference between the classical K-SVD method and our method. While K-SVD requires that we explicitly set the sparsity level, in our approach we affect sparsity implicitly through our formulation and via the regularization parameter λ .

We use the Alternating Direction Method of Multipliers (ADMM) (see e.g. [4]) to compute an approximate local minimizer of (3). Learning the dictionary with an ADMM method has the advantages that it is less dependent on the initial dictionary, and it changes the initial dictionary drastically during the first few steps. At the same time the updates are cheap to compute, making the method suited for large-scale problems. The implementation details are included in the Appendix.

3.2 The Reconstruction Problem

Recall that we formulate the tomographic reconstruction problem as $Ax \approx b$, where b contains the noisy data and A is the system matrix. The vector x represents an $M \times N$ image of absorption coefficients, and these coefficients must be nonnegative to have physical meaning. Hence we must impose a nonnegativity constraint on the solution. A simple/naive tomographic reconstruction problem for Gaussian noise could thus be formulated as

$$\min_x \frac{1}{2} \|Ax - b\|_2^2 \quad \text{s.t.} \quad x \in \mathbb{R}_+^n.$$

Referring to (2), the loss function \mathcal{L}_{rec} is represented by the residual's 2-norm and the non-negativity of the image is imposed as a prior. Due to the ill-posed nature of the underlying problem, the lack of other priors results in unsatisfactory result.

We now turn to the reconstruction problem based on the patch dictionary D and problem formulation (2). For ease of our presentation we assume that the image size is a multiple of the patch size. Since the patch dictionary images are generally much smaller than the desired reconstruction ($P \ll M$ and $Q \ll N$), we partition the image into an $(M/P) \times (N/Q)$ array of non-overlapping blocks or patches represented by the vectors $x_j \in \mathbb{R}^p$ for $j = 1, \dots, q = (M/P)(N/Q)$. The advantage of using non-overlapping blocks, compared to overlapping blocks, is that we avoid over-smoothing the image textures when averaging over the overlapping regions, and it requires less computing time.

Each block of x is expressed as a conic combination of dictionary images, and hence the dictionary prior is expressed as

$$\Pi x = W\alpha, \quad W = (I \otimes D), \quad \alpha \geq 0, \quad (4)$$

where Π is a permutation matrix, W is the global dictionary for the image, and

$$\alpha = \begin{pmatrix} \alpha_1 \\ \vdots \\ \alpha_q \end{pmatrix} \in \underbrace{\mathbb{R}^s \times \dots \times \mathbb{R}^s}_{q \text{ times}}$$

is a vector of coefficients for each of a total of q blocks. Thus, the dimension of α is $sq = sn/p$ which is equal to the product of the over-representation factor s/p and the number of pixels n in the image. The permutation matrix Π re-orders the vector x such that we reconstruct the image block by block.

In pursuit of a nonnegative image x , we impose the constraint that the vector α should be nonnegative. This implies that each block x_j of x lies inside a polyhedral cone

$$\mathcal{C} = \{Dz \mid z \in \mathbb{R}_+^s\} \quad (5)$$

where $\mathcal{C} \subseteq \mathbb{R}_+^p$ since the dictionary images are all nonnegative. This is illustrated in Figure 1. Clearly, if the dictionary contains the standard basis of \mathbb{R}^p , then \mathcal{C} is equivalent to the entire nonnegative orthant in \mathbb{R}^p . However, if the cone \mathcal{C} is a proper subset of \mathbb{R}_+^p , then not all nonnegative images have an exact representation in \mathcal{C} , and hence the constraints $x_j \in \mathcal{C}$ may have a regularizing effect even without a sparsity prior on α . This can also be motivated by the

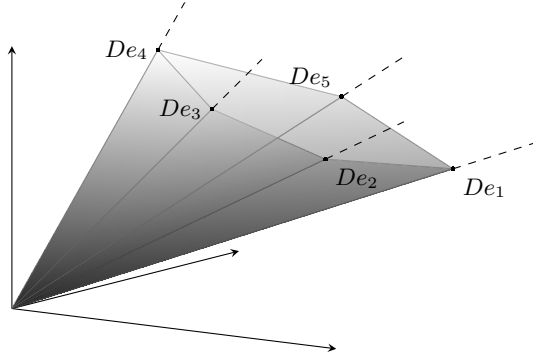


Figure 1: Polyhedral cone in \mathbb{R}_+^p spanned by five nonnegative dictionary elements, where e_i denotes the i th canonical unit vector in \mathbb{R}^s .

fact that the faces of the cone \mathcal{C} consist of images x_j that can be represented as a conic combination of at most $p - 1$ dictionary images.

Adding a sparsity prior on α , in addition to nonnegativity constraints, corresponds to the belief that x_j can be expressed as a conic combination of a small number of dictionary images and hence provides additional regularization. We include a 1-norm regularizer in our reconstruction problem as an approximate sparsity prior on α .

Reconstruction based on non-overlapping blocks often gives rise to block artifacts in the reconstruction because the objective in the reconstruction problem does not penalize jumps across the boundaries of neighboring blocks. To mitigate this type of artifact, we add a penalty term that discourages such jumps. We choose a penalty of the form

$$\psi(z) = \frac{1}{M(M/P - 1) + N(N/Q - 1)} \frac{1}{2} \|Lz\|_2^2 \quad (6)$$

where L is a matrix such that Lz is a vector with finite-difference approximations of the directional derivatives across the block boundaries. The denominator is the total number of pixels along the boundaries of the blocks in the image.

The constrained least squares reconstruction problem is then given by

$$\begin{aligned} & \text{minimize}_{\alpha} \quad \frac{1}{2} \frac{1}{m} \|A\Pi^T(I \otimes D)\alpha - b\|_2^2 + \mu \frac{1}{q} \|\alpha\|_1 + \delta^2 \psi(\Pi^T(I \otimes D)\alpha) \\ & \text{subject to} \quad \alpha \geq 0 \end{aligned} \quad (7)$$

with regularization parameters $\mu, \delta > 0$. We seek to make the problem formulation scale-invariant by i) division of the squared residual norm by the number of measurement m , ii) division of the 1-norm constraint by the number of blocks q , and iii) the scaling used in ψ (6).

Relaxing the non-negativity constraint or the 1-norm penalty on the representation vector α in (7) can be considered as a different choice of priors (less strong ones) under the same problem formulation assumptions in (2). The problem (7) is a convex but non-differentiable optimization problem which belongs to the class of sparse approximation problems, for which several algorithms have been developed recently (see [5] and [8] for details).

4 Numerical Experiments

In this section we use numerical examples to demonstrate and quantify the behavior of our two-stage algorithm and evaluate the computed reconstructions. In particular we explore the influence of the dictionary structure and its parameters (number of elements, patch sizes) on the reconstruction, in order to illustrate the role of the learned dictionary.

The underlying idea is to compute a regularized least squares fit in which the solution is expressed in terms of the dictionary, and hence it lies in the cone \mathcal{C} (5) defined by the dictionary elements. Hence there are two types of errors in the reconstruction process. Typically, the exact image does not lie in the cone \mathcal{C} , leading to an *approximation error*. Moreover, we encounter a *regularization error* due to the combination of the error present in the data and the regularization scheme.

In the learning stage we use a data set of images which are similar to the ones we wish to reconstruct. The ground-truth or exact image x^{exact} is not contained in the training set, so that we avoid committing an inverse crime. All images are gray-level and scaled in the interval $[0, 1]$.

For our highly underdetermined problems we know that both filtered back projection and algebraic iterative techniques give unsatisfactory solutions, and therefore we only compare our method with the TV reconstruction method. We use the discrete TV regularization problem formulation as

$$\min_{x \in \mathcal{Q}} \frac{1}{2} \|Ax - b\|_2^2 + \lambda_{\text{TV}} \sum_{1 \leq i \leq n} \|D_i^{\text{fd}} x\|_2 \quad (8)$$

where $\mathcal{Q} = \{x \in \mathbb{R}^n \mid 0 \leq x_i \leq 1\}$, D_i^{fd} computes a finite-difference approximation of the gradient at each pixel, and $\lambda_{\text{TV}} > 0$ is the TV regularization parameter.

All experiments were run in MATLAB (R2011b) on a 64-bit Linux system. The reconstruction problems are solved using the software package TFOCS (Templates for First-Order Conic Solvers) [2]. We compare with TV reconstructions computed by means of the MATLAB software TVREG [14].

4.1 The Test Image and the Tomographic Test Problem

The test images in Sections 4.2–4.5 are chosen as square patches from a high-resolution photo of peppers with uneven surfaces, making them interesting test images for studies of the reconstruction of textures. Figure 2 shows the 1600×1200 high-resolution image and the exact image of dimensions $M \times N = 200 \times 200$. This size allows us to perform many numerical experiments in a reasonable amount of time; we demonstrate the performance of our algorithm on a larger test problem in Section 4.6.

All test problems represent a parallel-beam tomographic measurement, and we use the function `parallel_tomo` from the MATLAB package AIR TOOLS [12] to compute the matrix A . The number of rays in each projection is given by $N_r = \lfloor \sqrt{2}N \rfloor$. If the total number of projections is N_p then the number of rows in A is $m = N_r N_p$ while the number of columns is $n = MN$. In particular we are interested in scenarios with a small number of projections. The exact data is generated with the forward model after which we add Gaussian white noise, i.e., $b = Ax^{\text{exact}} + e$.

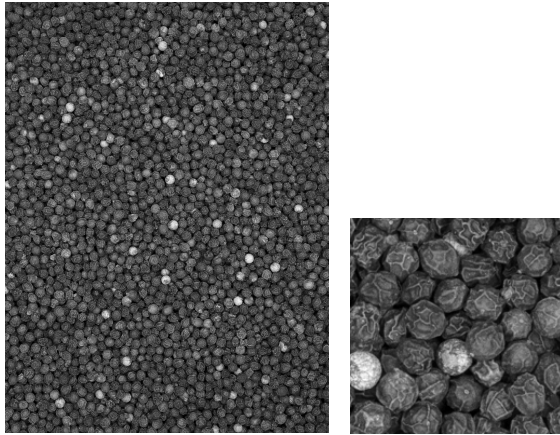


Figure 2: Left: the high-resolution image from which we obtain the training image patches. Right: the 200×200 exact image x^{exact} .

4.2 Studies of the Dictionary Learning Stage

It is not straightforward to evaluate the performance of the dictionary learning algorithm, considering that we are dealing with a non-convex optimization problem. In addition, the computed dictionary must be validated to estimate how well it will perform in practice. We are aware that the parameters of the dictionary learning algorithm can have a great impact on the obtained dictionary.

A good dictionary should preserve the structural information of the training images as much as possible and, at the same time, admit a sparse representation as well as a small factorization error. These requirements are related to the number of dictionary elements, i.e., the number of columns s in the matrix D . Since we want a compressed representation of the training images we choose s such that $p \leq s \ll t$, and the precise value will be investigated. The optimal patch size $P \times Q$ is unclear and will also be studied; without loss of generality we assume $P = Q$.

The regularization parameter λ in (3) balances the matrix factorization error and the sparsity constraint on the elements of the matrix H . The larger the λ , the more weight is given to minimization of $\|H\|_{\text{sum}}$, while for small λ more weight is given to minimization of the factorization error. If $\lambda = 0$ then (3) reduces to the classical nonnegative matrix factorization problem.

From the analysis of the upper bound on the regularization parameter λ in the Appendix, we know $\lambda \geq p$ implies $H = 0$; so λ can be varied in the interval $(0, p]$ to find dictionaries with different sparsity priors. Note that the scaling of the training images affects the scaling of the matrix H as well as the regularization parameter λ .

To evaluate the impact of the dictionary parameters, we use three different patch sizes (5×5 , 10×10 , and 20×20) and the number of dictionary elements s is chosen to be 2, 3, and 4 times the of the number of rows p in dictionary D .

The training patches are easy to acquire. We extract more than 50,000 patches from the high-resolution image in Figure 2, and for different combinations of patch sizes and number of dictionary elements we solve the dictionary

learning problem (3). Figure 3 shows examples of such learned dictionaries, where columns of D are represented as images; we see that the penalty constraint $D \in \mathcal{D}_\infty$ gives rise to “binary looking” dictionary elements while $D \in \mathcal{D}_2$ results in dictionary elements that use the whole gray-scale range.

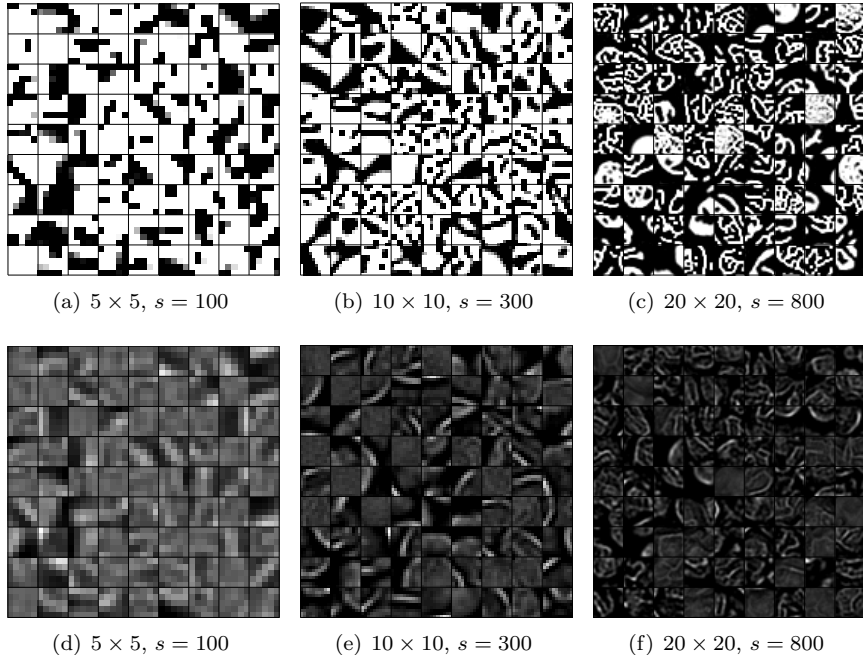


Figure 3: Examples of dictionary elements. Top row: with the constraint $D \in \mathcal{D}_\infty$ the images appear as “binary looking.” Bottom row: with the constraint $D \in \mathcal{D}_2$ the images appear to use the whole gray-scale range.

To evaluate the approximation error, i.e., the distance of the exact image x^{exact} to its projection on the cone \mathcal{C} (5), we compute the solutions α_j^* to the q approximation problems for all blocks $j = 1, 2, \dots, q$ in x^{exact} ,

$$\min_{\alpha_j} \frac{1}{2} \|D\alpha_j - x_j^{\text{exact}}\|_2^2 \quad \text{s.t.} \quad \alpha_j \geq 0. \quad (9)$$

Then $P_{\mathcal{C}}(x_j^{\text{exact}}) = D\alpha_j^*$ is the best representation/approximation of the j th block in the cone. The mean approximation error (MAE) is then computed as

$$\text{MAE} = \frac{1}{pq} \sum_{j=1}^q \|P_{\mathcal{C}}(x_j^{\text{exact}}) - x_j^{\text{exact}}\|_2. \quad (10)$$

In addition to the regularization parameter λ , the patch size as well as the number of dictionary elements determine how well the features and textures from the training images are represented in the dictionary (cf. Figure 3) and, hence, how good a reconstruction we are able to compute. Figure 4 shows how the mean approximation error MAE associated with the dictionary varies with patch size p , number of dictionary elements s , and regularization parameter λ . We see that MAE decreases as the patch size increases, so overall we tent to

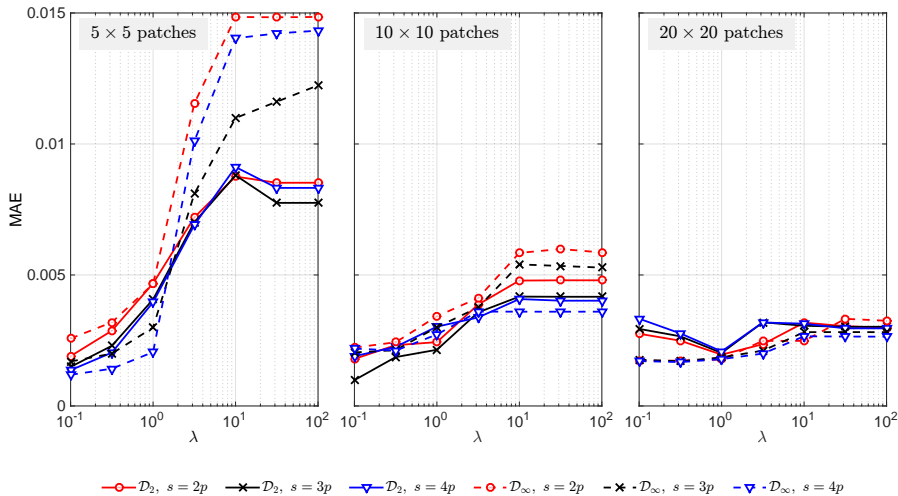


Figure 4: Mean approximation errors (10). Results for both $D \in \mathcal{D}_\infty$ and $D \in \mathcal{D}_2$ with different patch sizes and different s .

prefer larger patch sizes. A further advantage of larger patch sizes is that the variation of MAE with s and λ is less pronounced than for small patch sizes. In particular, for a large patch size we can use a smaller over-representation factor s/p than for a small patch size.

The computational work depends on the patch size and the number of dictionary elements which, in turn, affects the approximation error: the larger the dictionary, the smaller the approximation error, but at a higher computational cost. We have found that a good trade-off between the computational work and the approximation error can be obtained by increasing the number of dictionary elements until the approximation error levels off.

Let us return to the constraints $D \in \mathcal{D}_\infty$ and $D \in \mathcal{D}_2$. The average of the mean approximation error is lower for the gray-scale looking dictionary images in \mathcal{D}_2 with 5×5 and 10×10 patches, while the mean approximation error is smaller for the binary looking dictionary elements in \mathcal{D}_∞ with 20×20 patches. Consequently, with patch sizes 5×5 and 10×10 we expect smaller reconstruction errors with $D \in \mathcal{D}_2$ than with $D \in \mathcal{D}_\infty$. Furthermore, we can argue that for representing gray-scale patches (as in the reference image) with binary looking images in \mathcal{D}_∞ , a larger number of dictionary elements may be needed. So from now on, we choose $D \in \mathcal{D}_2$.

4.3 Studies of the Reconstruction Stage

Here we evaluate the overall reconstruction framework including the effect of the reconstruction parameters as well as their connection to the dictionary learning parameter λ and the patch size.

We solve the reconstruction problem (7) using the exact image given in Figure 2. We choose $N_p = 25$ projections corresponding to uniformly distributed angles in $[0^\circ, 180^\circ]$. Hence the matrix A has dimensions $m = \lfloor \sqrt{2} \cdot 200 \rfloor \cdot 25 = 7,075$ and $n = 200^2 = 40,000$, so the problem is highly underdetermined. We

use the relative noise level $\|e\|_2/\|Ax^{\text{exact}}\|_2 = 0.01$. Moreover, we use 5×5 , 10×10 and 20×20 patches and corresponding dictionary matrices $D^{(5)}$, $D^{(10)}$, and $D^{(20)}$ in \mathcal{D}_2 of size 25×100 , 100×300 , and 400×800 , respectively. The corresponding dictionary elements are shown in the bottom row of Figure 3.

We first investigate the reconstruction's sensitivity to the choice of λ in the dictionary learning problem and the parameters μ and δ in the reconstruction problem. To simplify the notation of (7) we define $\tau = \mu/q$. It follows from the optimality conditions of (7) that $\alpha^* = 0$ is optimal when $\tau \geq \bar{\tau} = \|\frac{1}{m}(I \otimes D^T)\Pi A^T b\|_\infty$ and hence we choose $\tau \in [0, \bar{\tau}]$. Later we see that we may be able to obtain good reconstructions for $\tau = 0$. Large values of τ refer to the case where the sparsity prior is strong and the solution is presented with too few dictionary elements. On the other hand if τ is small and a sufficient number of dictionary elements are included, the reconstruction error worsens only slightly when τ decreases.

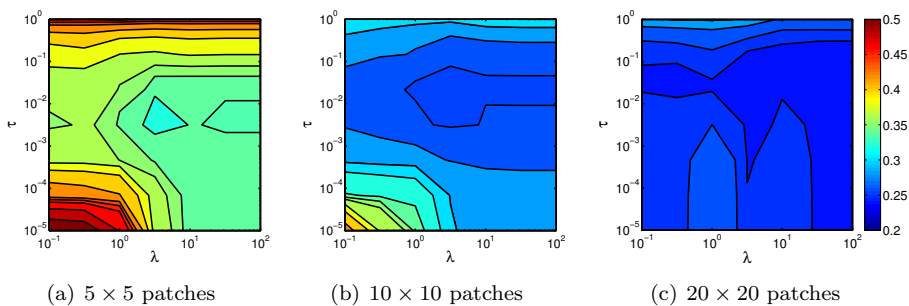


Figure 5: Contour plots of the reconstruction error RE (11) versus λ and $\tau = \mu/q$.

To investigate the effect of regularization parameters λ and τ , we first perform experiments with $\delta = 0$ corresponding to no image prior. The quality of a solution x is evaluated by the *reconstruction error*

$$\text{RE} = \|x - x^{\text{exact}}\|_2 / \|x^{\text{exact}}\|_2 \quad (11)$$

shown as contour plots in Figure 5. The reconstruction error is smaller for larger patch sizes, and also less dependent on the regularization parameters λ and τ . The smallest reconstruction errors are obtained in all dictionary sizes for $\lambda \approx 3$.

Let us now consider the reconstructions when $\delta > 0$ in order to reduce block artifacts. Figure 6 shows contour plots of the reconstruction errors versus τ and δ , using a fixed $\lambda = 3.16$. It is no surprise that introducing δ acts as a regularizer that can significantly improve the reconstruction. Sufficiently large values of δ yield smaller reconstruction errors. In consistence with the results from Figure 5 the reconstruction errors are smaller for 10×10 and 20×20 patch sizes than for 5×5 patches. For larger patch sizes (which allow for capturing more structure in the dictionary elements) the reconstruction error is quite insensitive to the choice of δ and τ . The contour plots in Figure 6 suggest that with our problem specification, $\delta \geq 1$ provide better reconstructions.

Finally, in Figure 7 we compare our reconstructions with those computed by means of TV regularization. To be fair, the TV regularization parameter was

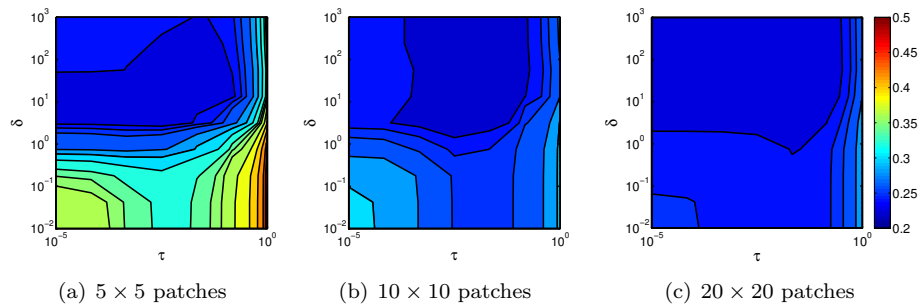


Figure 6: Contour plots of the reconstruction errors RE (11) versus $\tau = \mu/q$ and δ for a fixed $\lambda = 3.16$.

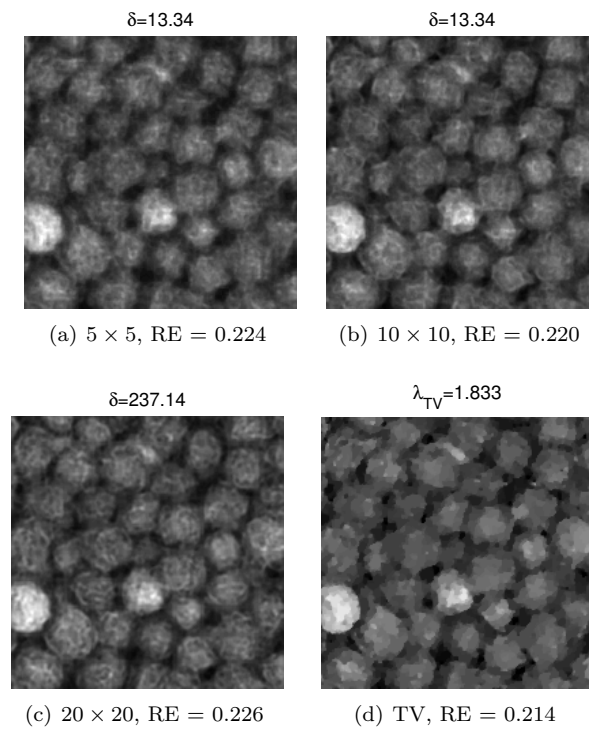


Figure 7: Reconstructions for different patch sizes, with $D \in \mathcal{D}_2$, $\lambda = 3.16$, and $\tau = 0.022$, compared with the TV solution. RE denotes the reconstruction error (11).

chosen to yield an optimal reconstruction. The reconstruction error for the TV solution is slightly smaller than that for our solutions, but despite of this our learned dictionary algorithm clearly gives solutions that are visually superior to the those obtained by TV because the latter method fails to capture the texture of the peppers. While using $D^{(10)}$ leads to the small 2-norm reconstruction error, the visually most appealing solution is obtained with $D^{(20)}$.

4.4 Simplifying the Computational Problem

We have been working under the assumption that $\alpha \geq 0$ and that it is sparse. Imposing both non-negativity and a 1-norm constraint on the representation vector α are strong assumptions in the reconstruction formulation.

If we relax the non-negativity constraint in the image reconstruction problem, then (7) can be reformulated as a constrained least squares problem:

$$\min_{\alpha} \frac{1}{2} \left\| \begin{pmatrix} \frac{1}{\sqrt{m}} A \Pi^T (I \otimes D) \\ \delta \psi(\Pi^T (I \otimes D)) \end{pmatrix} \alpha - \begin{pmatrix} b \\ 0 \end{pmatrix} \right\|_2^2 \quad \text{s.t.} \quad \|\alpha\|_1 \leq \gamma, \quad (12)$$

where $\gamma > 0$.

Alternatively we can relax the parameter τ . This is motivated by the plots in Figures 5 and 6 which suggest that for sufficiently large λ , δ and patch sizes, the reconstruction error is almost independent of τ as long as it is small. When $\tau = 0$ we exclude the 1-norm constraint on the representation vector α , and (7) reduces to a nonnegative constrained least square problem:

$$\min_{\alpha} \frac{1}{2} \left\| \begin{pmatrix} \frac{1}{\sqrt{m}} A \Pi^T (I \otimes D) \\ \delta \psi(\Pi^T (I \otimes D)) \end{pmatrix} \alpha - \begin{pmatrix} b \\ 0 \end{pmatrix} \right\|_2^2 \quad \text{s.t.} \quad \alpha \geq 0. \quad (13)$$

We use the same test problem with 25 projections and relative noise level 0.01 as in Section 4.3. We solve problem (12) for $D^{(10)} \in \mathcal{D}_2$, which resulted in the smallest reconstruction error when solving (7) (cf. Figure 7). Likewise we choose 10×10 and 20×20 patch sizes and $D^{(10)}, D^{(20)} \in \mathcal{D}_2$ to solve the nonnegatively constrained least square problem (13). Figures 8 and 9 show reconstructions when solving the two above problems (12) and (13), respectively.

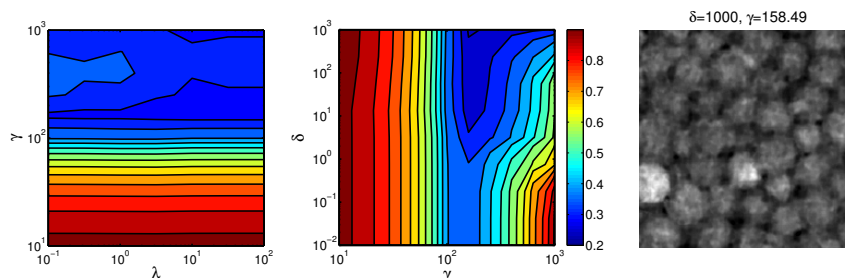


Figure 8: Contour plots of the reconstruction error RE for problem (12), similar to Figures 5 and 6. Left: RE versus λ and γ when $\delta = 0$. Middle: RE versus γ and δ with fixed $\lambda = 10$. Right: The best reconstruction with RE = 0.243.

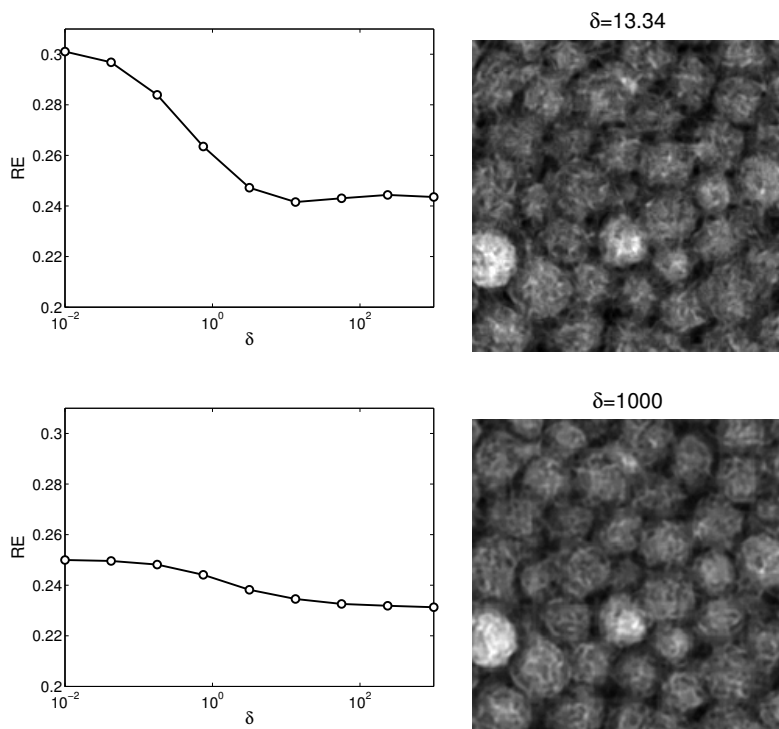


Figure 9: Left: plots of reconstruction error versus δ for problem (13), using fixed $\lambda = 3.16$ and $\tau = 0$. Right: the best reconstructions with $RE = 0.242$ and $RE = 0.231$. The top and bottom rows correspond to patch sizes 10×10 and 20×20 , respectively.

There are two problems with the reconstructions computed via (12). The lack of a nonnegativity constraint on α can lead to negative pixel values in the reconstruction, which are undesired. Also, as can be seen in Figure 8, the reconstruction is very sensitive to the choice of the regularization parameter γ ; it must be sufficiently large to allow the solution to be represented with a sufficient number of dictionary elements, and it should be carefully chosen to provide an acceptable reconstruction.

The solution to problem (13) for a 20×20 patch size, compared to the solution shown in Figure 7, is not significantly worse both visually and in terms of reconstruction error. This suggests that using the dictionary obtained from (3) with a proper choice of λ and patch size and a nonnegativity constraint may be sufficient for the reconstruction problem, i.e., we can let $\tau = 0$. While this seems to simplify the problem – going from (7) to (13) – it does not significantly simplify the computational optimization problem, since the 1-norm constraint is handled by simple thresholding in the software; but it helps us to get rid of a parameter in the reconstruction process. Also, when the 1-norm constraint is neglected one should be careful with the choice of λ and patch sizes, for otherwise irrelevant features and artifacts of noise may be introduced.

4.5 Studies of Sensitivity to Noise and Limited-Angle Data

To further study the performance of our algorithm, in this section we consider reconstructions based on (7) with more noise in the data, and with projections within a limited range. The first two sets use 25 and 50 projections with uniform angular sampling in $[0^\circ, 180^\circ]$ and with relative noise level = 0.05, i.e., a higher noise level than above. The reconstructions are shown in the top and middle rows of Figure 10. The reconstruction errors are still similar across the methods; however, the TV reconstructions have the characteristic “cartoonish” appearance while the dictionary-based reconstructions retain much of the structure and texture but have other artifacts – especially for $N_p = 25$. We also note that these artifacts are different for the two different dictionaries.

The third set uses 25 projections uniformly distributed in the limited range $[0^\circ, 120^\circ]$ and with relative noise level 0.01. In this case the TV reconstructions display additional artifacts related to the limited-angle situation, while such artifacts are less pronounced in the reconstructions by our algorithm.

4.6 A Large Test Case

We finish the numerical experiments with a verification of our method on two larger test problems that simulate the analysis of microstructure in materials science. Almost all common metals, and many ceramics, are polycrystalline, i.e., they are composed of many small crystals or grains of varying size and orientation, and the variations in orientation can be random. A grain boundary is the interface between two grains. It is of particular interest to study how these boundaries move over time, for instance when the material is exposed to external stimuli such as heat or pressure. Here we assume that priors of the grain structure are available in the form of training images.

The simulated data was computed using images of steel and zirconium grains. The steel microstructure image from [34] is of dimensions 900×1280 and the zirconium grain image (produced by a scanning electron microscope) is 760×1020 .

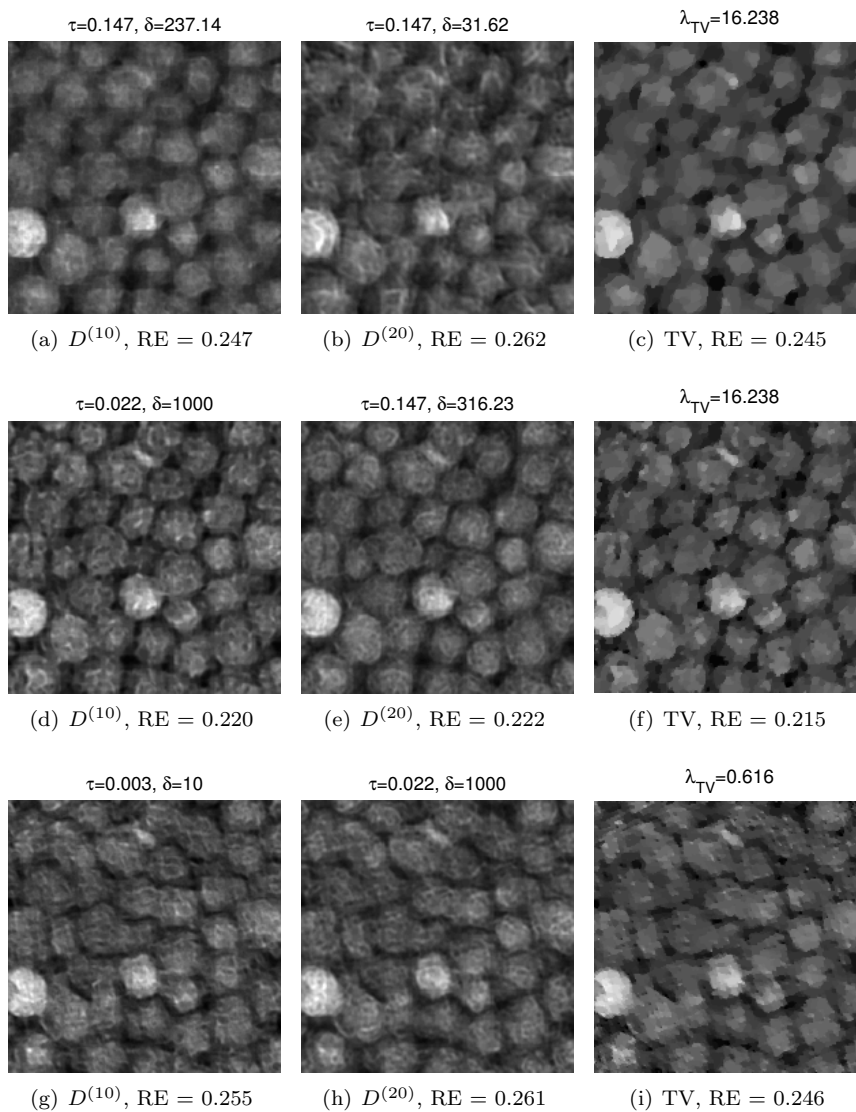


Figure 10: The left and middle columns show our reconstructions with $\lambda = 3.16$ using $D^{(10)}$ and $D^{(20)}$, respectively; the right column shows the TV reconstructions. Top and middle rows: $N_p = 25$ and $N_p = 50$ projections in $[0^\circ, 180^\circ]$ and relative noise level 0.05. Bottom row: $N_p = 25$ projections in $[0^\circ, 120^\circ]$ and relative noise level 0.01.

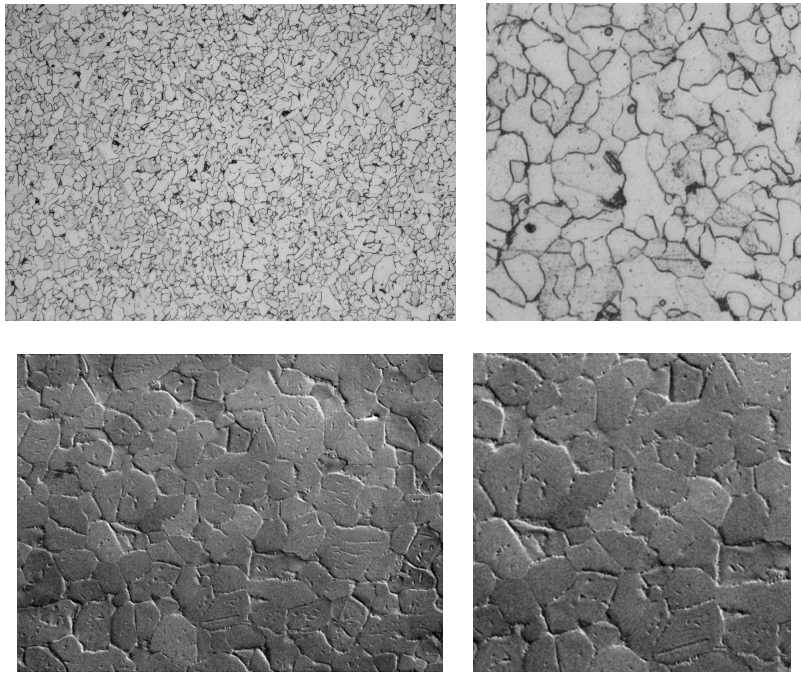


Figure 11: Left: high-resolution images of steel micro-structure [34] (top) and zirconium grains (bottom) used to generate the training images. Right: the corresponding exact images of size 520×520 .

More than 50,000 patches are extracted from these images to learn dictionaries $D^{(20)} \in \mathcal{D}_2, \mathcal{D}_\infty$ of size 400×800 . To avoid doing inverse crime, we obtain the exact images of dimensions 520×520 by first rotating the high-resolution image and then extracting the exact image. The high-resolution images and the exact images are shown in Figure 11.

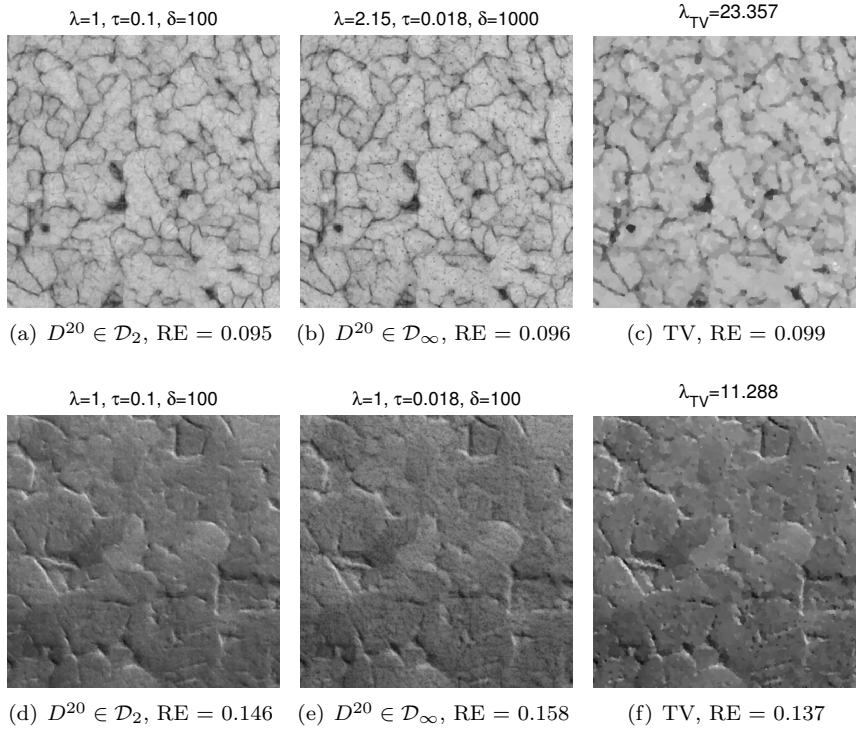


Figure 12: Reconstructions of the 520×520 images by our method (left and middle) and by the TV method (right). Top: steel microstructure. Bottom: zirconium grains.

We consider a parallel-beam tomographic scenario with $N_p = 50$ projections corresponding to 50 uniformly distributed projections in $[0^\circ, 180^\circ]$, leading to $m = 36,750$ data values. We add Gaussian white noise with relative noise level 0.01 and compute reconstructions by our method as well as the TV method; these reconstructions are shown in Figure 12. All regularization parameters were chosen to give the best reconstruction as measured by the RE, and we note that the reconstruction errors are dominated by the error coming from the regularization of the noisy data; the approximation errors $\|P_C(x^{\text{exact}}) - x^{\text{exact}}\|_2 / \|x^{\text{exact}}\|_2$ are of the order 0.03 and 0.05 for the steel and zirconium images, respectively.

We see that our algorithm, for both \mathcal{D}_2 and \mathcal{D}_∞ , performs better than the TV method for recovering the textures and, in particular, the grain boundaries that are of interest here. Our reconstructions for \mathcal{D}_∞ have the sharpest grain boundaries, but some small black “dots” have appeared which are not present for \mathcal{D}_2 ; in both cases the images are suited for postprocessing via image analysis.

5 Conclusions

In this paper we study how to incorporate training-images as priors in the tomographic image reconstruction problem via a two-stage framework. In the first stage we compute a learned dictionary from a set of training images using a constrained nonnegative matrix factorization (NNMF) (a nonnegative sparse coding problem). In the second stage, via a regularized least squares fit, we compute a nonnegative reconstruction lying in the cone defined by the dictionary elements; the reconstruction is sparse with respect to the dictionary.

Our algorithm includes several regularization parameters. In the first stage a parameter is used to control the sparsity in the NNMF, and in the second stage we use one parameter to control the sparsity of the representation in the dictionary, and another parameter to avoid blocking artifacts (because we work with non-overlapping image patches). Our numerical experiments demonstrate the interplay between these parameters and the computed reconstructions, and in particular we show that the reconstructions are not very sensitive to these parameters, and that they can be chosen from a few numerical experiments.

Our focus is on underdetermined problems where a strong prior is needed to compute a reliable reconstruction, and our experiments show that for images with structure or texture our algorithm is superior to total variation regularization (another method that incorporates a strong prior). Further work is needed to develop automatic algorithms for choosing the regularization parameters.

Acknowledgments

The authors would like to thank Prof. Samuli Siltanen from Univ. of Helsinki for providing the high-resolution image of the peppers, and Dr. Hamidreza Abdolvand from Univ. of Oxford for providing the zirconium image.

Appendix: The Dictionary Learning Algorithm

Recall that the dictionary learning problem (3) is non-convex, and hence it is too costly to solve it globally. We will therefore optimize locally by applying the Alternating Direction Method of Multipliers (ADMM) method [4] to the following reformulation of (3)

$$\begin{aligned} & \text{minimize}_{D,H} \quad \frac{1}{2} \|Y - UV\|_{\mathbb{F}}^2 + \lambda \|H\|_{\text{sum}} + I_{\mathbb{R}_+^{s \times t}}(H) + I_{\mathcal{D}}(D) \\ & \text{subject to} \quad D = U, H = V, \end{aligned} \quad (14)$$

where $U \in \mathbb{R}^{p \times s}$ and $V \in \mathbb{R}^{s \times t}$ are auxiliary variables that are introduced in order to make the ADMM-updates separable and hence cheap. The augmented Lagrangian associated with (14) can be expressed as

$$\begin{aligned} L_{\rho}(D, H, U, V, \Lambda, \Pi) = & \frac{1}{2} \|Y - UV\|_{\mathbb{F}}^2 + \lambda \|H\|_{\text{sum}} + I_{\mathbb{R}_+^{s \times t}}(H) + I_{\mathcal{D}}(D) \\ & + \text{Tr}(\Lambda^T (D - U)) + \text{Tr}(\Pi^T (H - V)) \\ & + \frac{\rho}{2} \|D - U\|_{\mathbb{F}}^2 + \frac{\rho}{2} \|H - V\|_{\mathbb{F}}^2 \end{aligned} \quad (15)$$

where $\Lambda \in \mathbb{R}^{p \times s}$ and $\Pi \in \mathbb{R}^{s \times l}$ are Lagrange multipliers, and ρ is a positive penalty parameter which can be chosen fixed prior to the learning process. If we partition the variables into two blocks (D, V) and (H, U) and apply ADMM to (14), we obtain an algorithm where each iteration involves the following three steps: (i) minimize L_ρ jointly over D and V ; (ii) minimize L_ρ jointly over H and U ; and (iii) update the dual variables Λ and Π by taking a gradient-ascent step. Since L_ρ is separable in D and V , step (i) can be expressed as two separate updates

$$D_{k+1} = \min_{D \in \mathcal{D}} L_\rho(D, H_k, U_k, V_k, \Lambda_k, \Pi_k) = P_{\mathcal{D}}(U_k - \rho^{-1} \Lambda_k) \quad (16a)$$

$$\begin{aligned} V_{k+1} &= \min_V L_\rho(D_k, H_k, U_k, V, \Lambda_k, \Pi_k) \\ &= (U_k^T U_k + \rho I)^{-1} (U_k^T Y + \Pi_k + \rho H_k) \end{aligned} \quad (16b)$$

where $P_{\mathcal{D}}(\cdot)$ is the projection onto the set \mathcal{D} . Similarly, L_ρ is also separable in H and U , so step (ii) can be written as

$$H_{k+1} = \min_{H \in \mathbb{R}_+^{s \times t}} L_\rho(D_{k+1}, H, U_k, V_{k+1}, \Lambda_k, \Pi_k) \quad (16c)$$

$$\begin{aligned} &= P_{\mathbb{R}_+^{s \times t}}(\mathcal{S}_{\lambda/\rho}(V_{k+1} - \rho^{-1} \Pi_k)) \\ U_{k+1} &= \min_U L_\rho(D_{k+1}, H_k, U, V_{k+1}, \Lambda_k, \Pi_k) \\ &= (Y V_{k+1}^T + \Lambda_k + \rho D_{k+1})(V_{k+1} V_{k+1}^T + \rho I)^{-1} \end{aligned} \quad (16d)$$

where $\mathcal{S}_{\lambda/\rho}$ denotes an entrywise soft-thresholding operator, and $P_{\mathbb{R}_+^{s \times t}}(\cdot)$ is the projection onto the non-negative orthant. Finally, the dual variable updates in step (iii) are given by

$$\Lambda_{k+1} = \Lambda_k + \rho(D_{k+1} - U_{k+1}) \quad (16e)$$

$$\Pi_{k+1} = \Pi_k + \rho(H_{k+1} - V_{k+1}). \quad (16f)$$

The projection onto the set \mathcal{D}_∞ is an element-wise projection onto the interval $[0, 1]$ and hence easy to compute. However, the projection onto \mathcal{D}_2 does not have a closed form solution, so we compute it iteratively using Dykstra's alternating projection algorithm.

The convergence properties of ADMM when applied to non-convex problems of the form (14) have been studied by e.g. [33]. They show that whenever the sequence of iterates produced by (16) converges, the limit satisfies the the KKT-conditions (i.e., the first-order necessary conditions for optimality) which can be expressed as

$$\begin{aligned} D &= U, & H &= V, \\ A &= -(Y - DH)H^T, & \Pi &= -D^T(Y - DH), \\ -A &\in \partial\Phi_{\text{dic}}(D), & -\Pi &\in \lambda \partial\Phi_{\text{rep}}(H). \end{aligned}$$

The convergence result is somewhat weak, but empirical evidence suggests that applying ADMM to non-convex problems often works well in practice [4]. It is interesting to note that the point $D = U = 0$ and $H = V = 0$ satisfies the KKT-conditions, and although it is a stationary point, it is clearly not a local minima. For this reason, we avoid initializing with zeros. We initialize U with

some of the images in the training set and $V = H$ as the identity matrix of appropriate size.

The KKT-conditions can also be used to formulate stopping criteria. We use the following conditions

$$\frac{\|D - U\|_{\max}}{\max(1, \|D\|_{\max})} \leq \epsilon \quad \wedge \quad \frac{\|H - V\|_{\max}}{\max(1, \|H\|_{\max})} \leq \epsilon \quad (17a)$$

$$\frac{\|II - D^T(DH - Y)\|_{\max}}{\max(1, \|II\|_{\max})} \leq \epsilon \quad \wedge \quad \frac{\|A - (DH - Y)H^T\|_{\max}}{\max(1, \|A\|_{\max})} \leq \epsilon \quad (17b)$$

where $\epsilon > 0$ is a given tolerance.

The KKT-conditions can also be used to derive an upper bound $\bar{\lambda}$ for the regularization parameter λ . Specifically, if for some $\bar{\lambda}$ and all $D \in \mathcal{D}$ we have

$$D^T Y \in \bar{\lambda} \partial \Phi_{\text{rep}}(0),$$

then $H = 0$ is also optimal for all $\lambda \geq \bar{\lambda}$. If all entries in Y are between 0 and 1, then the upper bound $\bar{\lambda} = p$ can be used for both dictionaries since

$$\sup_{D \in \mathcal{D}_2} \|D^T Y\|_{\max} = \max_{j=1, \dots, t} \sqrt{p} \|Y e_j\|_2 \leq p$$

and

$$\sup_{D \in \mathcal{D}_{\infty}} \|D^T Y\|_{\max} = \max_{j=1, \dots, t} \|Y e_j\|_1 \leq p$$

which implies that $D^T Y \in \bar{\lambda} \partial \Phi_{\text{rep}}(0)$ for all $D \in \mathcal{D}$.

References

- [1] M. Aharon, M. Elad, and A. Bruckstein, *K-SVD: an algorithm for designing overcomplete dictionaries for sparse representation*, IEEE Trans. Signal Process., **54** (2006), 4311–4322.
- [2] S. Becker, E. J. Candès and M. Grant, *Templates for convex cone problems with applications to sparse signal recovery*, Math. Prog. Comp., **3** (2011), 165–218.
- [3] J. Bian, J. H. Siewerdsen, X. Han, E. Y. Sidky, J. L. Prince, C. A. Pelizzari, and X. Pan, *Evaluation of sparse-view reconstruction from flat-panel-detector cone-beam CT*, Phys. Med. Biol., **55** (2010), 6575–6599.
- [4] S. Boyd, N. Parikh, E. Chu, B. Peleato, and J. Eckstein, *Distributed optimization and statistical learning via the alternating direction method of multipliers*, Foundations and Trends in Machine Learning, **3** (2011), 1–122.
- [5] A. M. Bruckstein, D. L. Donoho, and M. Elad, *From sparse solutions of systems of equations to sparse modeling of signals and images*, SIAM Review, **51** (2009), 34–81.
- [6] Y. Chen, Xi. Yin, L. Shi, H. Shu, L. Luo, J. L. Coatrieux and C. Toumoulin, *Improving abdomen tumor low-dose CT images using a fast dictionary learning based processing*, Phys. Med. Biol., **58** (2013), 5803–5820.

- [7] S. S. Chen, D. L. Donoho, M. A. Saunders, *Atomic decomposition by basis pursuit*, SIAM Review, **43** (2001), 129–159.
- [8] M. Elad, *Sparse and redundant representations, from theory to applications in signal and image processing*, Springer, New York, 2010.
- [9] M. Elad, and M. Aharon, *Image denoising via sparse and redundant representations over learned dictionaries* IEEE Trans. Image Process., **15** (2006), 3736–3745.
- [10] K. Engan, S. O. Aase, and J. H. Husøy, *Multi-frame compression: theory and design*, EURASIP Signal Process., **80** (2000), 2121–2140.
- [11] V. Etter, I. Jovanović, and M. Vetterli, *Use of learned dictionaries in tomographic reconstruction*, Proc. SPIE **8138**, Wavelets and Sparsity XIV (2011) 81381C.
- [12] P. C. Hansen and M. Saxild-Hansen, *AIR Tools – A MATLAB package of algebraic iterative reconstruction methods*, J. Comput. Appl. Math., **236** (2012), 2167–2178.
- [13] P. O. Hoyer, *Non-negative matrix factorization with sparseness constraints*, J. Mach. Learn. Res., **5** (2004), 1457–1469.
- [14] T. L. Jensen, J. H. Jørgensen, P. C. Hansen and S. H. Jensen, *Implementation of an optimal first-order method for strongly convex total variation regularization*, BIT, **52** (2011), 329–356.
- [15] A. Coates and A. Y. Ng, Learning feature representations with K-means, *Neural Networks: Tricks of the Trade*, (Eds. G. Montavon, G. B. Orr, K.-R. Müller), 2nd edn, Springer LNCS 7700, (2012), 561–580.
- [16] K. Kreutz-Delgado, J. F. Murray, B. D. Rao, K. Engan, T. Lee, and T. J. Sejnowski, *Dictionary learning algorithms for sparse representation*, Neural Comp., **15** (2003), 349–396.
- [17] S. J. LaRoque, E. Y. Sidky, and Xi. Pan, *Accurate image reconstruction from few-view and limited-angle data in diffraction tomography*, J. Opt. Soc. Am. A Opt. Image Sci. Vis., **25** (2008), 1772–1782.
- [18] D. D. Lee, and H. S. Seung, *Learning the parts of objects by non-negative matrix factorization*, Nature, **401** (1999), 788–791.
- [19] M.S.Lewicki and T.J. Sejnowski, *Learning overcomplete representations*, Neural Comp., **12** (2000), 337–365.
- [20] Sh. Li, L. Fang and H. Yin, *An efficient dictionary learning algorithm and its application to 3-D medical image denoising*, IEEE Trans. Biomed. Eng., **59** (2012), 417–427.
- [21] H. Y. Liao, and G. Sapiro, *Sparse representations for limited data tomography*, Proc. IEEE Int Symp. Biomed. Imaging, (2008), 1375–1378.
- [22] Q. Liu, D. Liang, Y. Song, J. Luo, Y. Zhu, and W. Li, *Augmented Lagrangian-based sparse representation method with dictionary updating for image deblurring*, SIAM J. Imaging Sci., **6** (2013), 1689–1718.

- [23] J. Mairal, G. Sapiro, and M. Elad, *Learning multiscale sparse representations for image and video restoration*, SIAM Multiscale Model. Simul., **7** (2008), 214–241.
- [24] J. Mairal, F. Bach, J. Ponce and G. Sapiro, *Online learning for matrix factorization and sparse coding*, J. Mach. Learn. Res., **11** (2010), 19–60.
- [25] B. A. Olshausen, and D. J. Field, *Emergence of simple-cell receptive field properties by learning a sparse code for natural images*, Nature, **381** (1996), 607–609.
- [26] S. Ravishankar, and Y. Bresler, *MR image reconstruction from highly undersampled k-space data by dictionary learning*, IEEE Trans. Med. Imag., **30** (2011), 1028–1041.
- [27] D. Strong, and T. Chan, *Edge-preserving and scale-dependent properties of total variation regularization*, Inverse Problems, **19** (2003), S165–S187.
- [28] R. Tibshirani, *Regression shrinkage and selection via the lasso*, J. R. Stat. Soc. Ser. B Stat. Methodol., **58** (1996), 267–288.
- [29] I. Tošić, I. Jovanović, P. Frossard, M. Vetterli, and N. Duric, *Ultrasound tomography with learned dictionaries*, IEEE Int. Conf. Acoust., Speech, Signal Processing, (2010), 5502–5505.
- [30] J. A. Tropp, and S. J. Wright, *Computational methods for sparse solution of linear inverse problems*, Proc. IEEE, **98** (2010), 948–958.
- [31] J. Velikina, Sh. Leng, and G. H. Chen, *Limited view angle tomographic image reconstruction via total variation minimization*, Proc. SPIE **6510**, *Medical Imaging 2007: Physics of Medical Imaging*.
- [32] Q. Xu, H. Yu, X. Mou, L. Zhang, J. Hsieh, and G. Wang, *Low-dose X-ray CT reconstruction via dictionary learning*, IEEE Trans. Med. Imag., **31** (2012), 1682–1697.
- [33] Y. Xu, W. Yin, Z. Wen and Y. Zhang, *An alternating direction algorithm for matrix completion with nonnegative factors*, Front. Math. China, **7** (2012), 365–384.
- [34] www.one-eighty-degrees.com/service/microstructural-investigations.